

## Optical properties of ZnSe

Sadao Adachi

*Department of Electronic Engineering, Faculty of Engineering, Gunma University, Kiryu-shi, Gunma 376, Japan*

Tsunemasa Taguchi

*Department of Electrical Engineering, Faculty of Engineering, Osaka University, Suita-shi, Osaka 565, Japan*

(Received 5 November 1990)

We have studied the optical response of ZnSe in the 1.5–5.3-eV photon-energy range at room temperature by spectroscopic ellipsometry. The measured dielectric-function spectra reveal distinct structures at energies of the  $E_0$ ,  $E_0 + \Delta_0$ ,  $E_1$ , and  $E_1 + \Delta_1$  critical points (CP's). These data are analyzed on the basis of a simplified model of the interband transitions. The  $E_0$ -( $E_0 + \Delta_0$ ) structures are characterized by a three-dimensional  $M_0$  CP, the  $E_1$ -( $E_1 + \Delta_1$ ) structures by a two-dimensional  $M_0$  CP, and the  $E_2$  structure by a classical Lorentzian oscillator (damped harmonic oscillator). The experimental data could not be explained within the framework of the one-electron approximation, since excitonic effects may profoundly modify the CP singularity structure. The model is thus made to account for the excitonic effects at these CP's; our results are in satisfactory agreement with the experiment over the entire range of photon energies. Dielectric-function-related optical constants of ZnSe, such as the refractive index, the extinction coefficient, and the absorption coefficient, are also presented and analyzed.

### I. INTRODUCTION

Although ZnSe is an attractive semiconductor as a material for optoelectronic devices, little is known about the optical response of this material at high photon energies.<sup>1–7</sup> For device applications, knowledge of the optical response over a wide energy range is of great importance.

Spectroscopic ellipsometry is an excellent technique for the investigation of the optical response of semiconductors<sup>8</sup> and has been used to study Si,<sup>9,10</sup> Ge,<sup>9,11</sup> Si<sub>x</sub>Ga<sub>1-x</sub>,<sup>12</sup>  $\alpha$ -Sn,<sup>13</sup> most III-V semiconductors,<sup>9,14–20</sup> CdSe,<sup>21</sup> Cd<sub>1-x</sub>Mn<sub>x</sub>Te,<sup>22</sup> and Cd<sub>x</sub>Hg<sub>1-x</sub>Se.<sup>23</sup> On-line digitization of the data permits fast and efficient analysis of the structure observed in the  $\epsilon(\omega)$  spectra in terms of standard analytical line shapes for interband critical points (CP's). Numerical differentiation of the data facilitates this analysis. However, to our knowledge, to date no spectroscopic-ellipsometry study has been carried out on ZnSe crystals.

In this paper we present the dielectric-function spectra of ZnSe at room temperature between 1.5 and 5.3 eV obtained from a numerical analysis of ellipsometry measurements. A method is also described for calculating the spectral dependence of the dielectric function,  $\epsilon(\omega) = \epsilon_1(\omega) + i\epsilon_2(\omega)$ , of ZnSe at energies below and above the lowest band gap, in which the model is based on the Kramers-Kronig (KK) transformation and strongly connected with the electronic energy-band structure of the medium.

### II. THEORETICAL MODEL

#### A. Electronic energy-band structure of ZnSe

A wide variety of calculations<sup>24–25</sup> and experiments<sup>1–7,36–44</sup> have yielded detailed information on the

electronic energy-band structure of ZnSe. We reproduce in Fig. 1 the energy-band structure of ZnSe as calculated by Chelikowsky and Cohen (Ref. 28) with an empirical-nonlocal-pseudopotential method. The electronic states are labeled with use of a notation for the double-group representations of the zinc-blende structure ( $F\bar{4}3m$  space group). The locations of several interband transitions are also included in the figure. These are the transitions which may play an important part in the analysis of optical spectra. We also list in Table I some CP energies and peak positions of the main structures present in the optical spectra of ZnSe (300 K) taken from the literature.

The fundamental absorption edge of ZnSe corresponds to direct transitions from the highest valence band to the lowest conduction band at the  $\Gamma$  point (i.e.,  $\Gamma_{15}^v \rightarrow \Gamma_1^c$ , in single-group notation). The spin-orbit interaction splits the  $\Gamma_{15}^v$  valence band into  $\Gamma_8^v$  and  $\Gamma_7^v$  (splitting energy,  $\Delta_0$ ) and the  $\Gamma_{15}^c$  conduction band into  $\Gamma_7^c$  and  $\Gamma_8^c$  (splitting energy,  $\Delta'_0$ ). The corresponding optical transitions at or near  $\mathbf{k}=0$  ( $\Gamma$ ) are, respectively, labeled  $E_0$  [ $\Gamma_8^v(\Gamma_{15}^v) \rightarrow \Gamma_6^c(\Gamma_1^c)$ ],  $E_0 + \Delta_0$  [ $\Gamma_7^v(\Gamma_{15}^v) \rightarrow \Gamma_6^c(\Gamma_1^c)$ ],  $E'_0$ , [ $\Gamma_8^v(\Gamma_{15}^v) \rightarrow \Gamma_7^c(\Gamma_{15}^c)$ ],  $E'_0 + \Delta_0$  [ $\Gamma_7^v(\Gamma_{15}^v) \rightarrow \Gamma_7^c(\Gamma_{15}^c)$ , dipole forbidden],  $E'_0 + \Delta'_0$  [ $\Gamma_8^v(\Gamma_{15}^v) \rightarrow \Gamma_8^c(\Gamma_{15}^c)$ ], and  $E'_0 + \Delta'_0 + \Delta_0$  [ $\Gamma_7^v(\Gamma_{15}^v) \rightarrow \Gamma_8^c(\Gamma_{15}^c)$ ]. A further  $E'_0$  transition, found in the calculation,<sup>28</sup> is located along [100] ( $\Delta$ ) about 60% of the way from  $\Gamma$  to  $X$ .

The spin-orbit interaction also splits the  $L_3^v$  ( $\Lambda_3^v$ ) valence band into  $L_{4,5}^v$  ( $\Lambda_{4,5}^v$ ) and  $L_6^v$  ( $\Lambda_6^v$ ) and the  $L_3^c$  ( $\Lambda_3^c$ ) conduction band into  $L_6^c$  ( $\Lambda_6^c$ ) and  $L_{4,5}^c$  ( $\Lambda_{4,5}^c$ ). The corresponding transitions are, respectively, labeled  $E_1$  [ $L_{4,5}^v(L_3^v) \rightarrow L_6^c(L_1^c)$  or  $\Lambda_{4,5}^v(\Lambda_3^v) \rightarrow \Lambda_6^c(\Lambda_1^c)$ ],  $E_1 + \Delta_1$  [ $L_6^v(L_3^v) \rightarrow L_6^c(L_1^c)$  or  $\Lambda_6^v(\Lambda_3^v) \rightarrow \Lambda_6^c(\Lambda_1^c)$ ],  $E'_1$  [ $L_{4,5}^v(L_3^v) \rightarrow L_6^c(L_3^c)$  or  $\Lambda_{4,5}^v(\Lambda_3^v) \rightarrow \Lambda_6^c(\Lambda_3^c)$ ], and  $E'_1 + \Delta'_1$  [ $L_{4,5}^v(L_3^v) \rightarrow L_{4,5}^c(L_3^c)$  or  $\Lambda_{4,5}^v(\Lambda_3^v) \rightarrow \Lambda_{4,5}^c(\Lambda_3^c)$ ].



calculations suggest that the indirect transitions in ZnSe occur in the spectral region close to the dominant  $E_1$  structure. Since the indirect transitions are higher-order perturbations than the direct ones, their strengths are usually very weak. As a result, their exceedingly weak nature would be completely overwhelmed by the  $E_1$ -gap contribution. We shall therefore not consider the contribution of the indirect transitions in the present analysis.

## B. Model dielectric function

The dielectric behavior of crystalline material is known to be strongly connected with its energy-band structure. Transitions involving these energy bands give rise to all the structure in the optical constants at readily accessible photon energies  $E = \hbar\omega$ . In our model, the dielectric function  $\epsilon(\omega)$  is approximated as a sum of several terms, each of which is an explicit function of energy and represents the contribution from the neighborhood of a CP in the joint density of states. These CP's are associated with transitions in the energy-band structure at the energies labeled  $E_0$ ,  $E_0 + \Delta_0$ ,  $E_1$ ,  $E_1 + \Delta_1$ , and  $E_2$ . In the following, we summarize specific expressions for  $\epsilon(\omega)$  [ $\epsilon_1(\omega) = \text{Re}\epsilon(\omega)$ ;  $\epsilon_2(\omega) = \text{Im}\epsilon(\omega)$ ] from these CP's (also see Refs. 45–51). As required,  $\epsilon_1(\omega)$  and  $\epsilon_2(\omega)$  are Kramers-Kronig transforms of each other.

### 1. $E_0$ and $E_0 + \Delta_0$ transitions

The  $E_0$ -( $E_0 + \Delta_0$ ) transitions are three-dimensional (3D)  $M_0$  CP's and occur in ZnSe at photon energies  $\sim 2.7$  eV ( $E_0$ ) and  $\sim 3.1$  eV ( $E_0 + \Delta_0$ ) at 300 K. Assuming the bands are parabolic, we obtain the contribution of these gaps to  $\epsilon(\omega)$ :

$$\epsilon(\omega) = AE_0^{-1.5} \{ f(\chi_0) + \frac{1}{2} [E_0 / (E_0 + \Delta_0)]^{1.5} f(\chi_{s.o.}) \}, \quad (1)$$

with

$$f(\chi_0) = \chi_0^{-2} [2 - (1 + \chi_0)^{0.5} - (1 - \chi_0)^{0.5}], \quad (2a)$$

$$f(\chi_{s.o.}) = \chi_{s.o.}^{-2} [2 - (1 + \chi_{s.o.})^{0.5} - (1 - \chi_{s.o.})^{0.5}], \quad (2b)$$

$$\chi_0 = (\hbar\omega + i\Gamma) / E_0, \quad (2c)$$

$$\chi_{s.o.} = (\hbar\omega + i\Gamma) / (E_0 + \Delta_0). \quad (2d)$$

In Eqs. (1) and (2)  $A$  and  $\Gamma$  are, respectively, the strength and broadening parameters of the  $E_0$ -( $E_0 + \Delta_0$ ) transitions.

It is well known that the discrete lines and continuum excitons in the neighborhood of the lowest direct band edge (3D  $M_0$  CP) drastically change the optical spectrum.<sup>52</sup> The discrete series of exciton lines at the  $E_0$ -( $E_0 + \Delta_0$ ) gaps can be simply given with Lorentzian line shape by

$$\epsilon(\omega) = \sum_{n=1}^{\infty} \frac{A_{0x}}{n^3} \left[ \frac{1}{E_0 - G_0/n^2 - \hbar\omega - i\Gamma} + \frac{1}{2} \left[ \frac{1}{E_0 + \Delta_0 - G_0/n^2 - \hbar\omega - i\Gamma} \right] \right], \quad (3)$$

where  $A_{0x}$  is the exciton strength parameter and  $G_0$  is the exciton binding energy [ $G_0 = 17$  meV (Ref. 53)]. Notice that the  $A_{0x}$  [also  $A$  in Eq. (1)] and  $G_0$  are, in principle, functions of the band parameter (i.e., the effective masses). In Eqs. (1) and (3) the  $\Gamma_7^-$ -band mass is assumed to be the same as the  $\Gamma_8^-$ -band mass. The expressions are, thus, not valid in the strict sense, but they are found to be a good approximation in practice.<sup>45–50,54</sup>

The continuum-exciton transitions at the 3D  $M_0$  CP behave like the noninteracting electron-hole pair characteristics. We therefore consider the contribution of these transitions to  $\epsilon(\omega)$  by expression (1).

### 2. $E_1$ and $E_1 + \Delta_1$ transitions

The  $E_1$  and  $E_1 + \Delta_1$  CP's may be of the 3D  $M_1$  type and occur in ZnSe at energies around  $\sim 5$  eV. Since the  $M_1$  CP longitudinal effective mass is much larger than its transverse counterparts, one can treat these 3D  $M_1$  CP's as a two-dimensional (2D) minimum  $M_0$ . The contribution to  $\epsilon(\omega)$  of the 2D minimum is given by

$$\epsilon(\omega) = -B_1 \chi_{1d}^{-1} \ln(1 - \chi_{1d}^2) - B_2 \chi_{1sd}^{-2} \ln(1 - \chi_{1sd}^2), \quad (4)$$

with

$$\chi_1 = (\hbar\omega + i\Gamma) / E_1, \quad (5a)$$

$$\chi_{1sd} = (\hbar\omega + i\Gamma) / (E_1 + \Delta_1), \quad (5b)$$

where the  $B$ 's and  $\Gamma$  are, respectively, the strength and broadening parameters of these transitions.

Equation (4) is a consequence of the one-electron approximation. Excitonic states should, in principle, exist at each type of CP, since the Coulomb-like interaction is always present between the electrons and the holes.<sup>55–61</sup> There may be only two analytical equations which enable us to treat the excitonic effects in the  $E_1$  to  $E_1 + \Delta_1$  spectral region: (1) the effective-mass (EM) approximation,<sup>55,56</sup> and (2) the Koster-Slater (KS) method.<sup>57,60</sup> Both the EM approximation and the KS method dramatically modify and sharpen the  $E_1$ -( $E_1 + \Delta_1$ ) structures of semiconductors.<sup>50</sup> We can, however, find a better fit with experiment using the EM approximation than the KS method.<sup>48,50</sup>

In the case of 3D  $M_1$  CP's (i.e., the saddle-point excitons or hyperbolic excitons), the EM equation is much more difficult to solve. However, in the approximation of the 2D  $M_0$  CP the equation gives a series of 2D Wannier-type excitons (discrete excitons).<sup>55</sup> The contribution of these excitons to  $\epsilon(\omega)$  can now be written with Lorentzian line shape as

$$\epsilon(\omega) = \sum_{n=1}^{\infty} \frac{1}{(2n-1)^3} \times \left[ \frac{B_{1x}}{E_1 - G_1 / (2n-2)^2 - \hbar\omega - i\Gamma} + \frac{B_{2x}}{E_1 + \Delta_1 - G_1 / (2n-1)^2 - \hbar\omega - i\Gamma} \right], \quad (6)$$

where the  $B_{1x}$  and  $B_{2x}$  are the 2D-exciton strength parameters at the  $E_1$  and  $E_1 + \Delta_1$  saddle points, respectively, and  $G_1$  is the 2D-exciton binding energy. The 2D EM approximation also gives a continuum part of the excitonic states.<sup>55</sup> However, one can consider that the contribution of this part is similar to that of the one-electron approximation [i.e., Eq. (4)].

### 3. $E_2$ transitions

The pronounced structure found in the optical spectra of ZnSe in the region higher in energy than  $E_1 + \Delta_1$  can be labeled  $E_2$  ( $\sim 6.7$  eV). The nature of the  $E_2$  transitions is complicated since they do not correspond to a single, well-defined CP.<sup>5,6,28</sup> Because of this, we shall characterize the  $E_2$  structure as that of a damped harmonic oscillator (DHO):

$$\epsilon(\omega) = \frac{C}{(1 - \chi_2^2) - i\chi_2\gamma}, \quad (7)$$

with

$$\chi_2 = \hbar\omega / E_2, \quad (8)$$

where  $C$  is the strength parameter and  $\gamma$  is the nondimensional broadening parameter.

## III. EXPERIMENT

The ZnSe samples used were single crystalline, not intentionally doped, and of high resistivity. They were grown by a recrystallization traveling-heater method (RTHM).<sup>62</sup> The method falls under the category of a THM, but should be distinguished from the THM in that polycrystalline ZnSe is charged into a capsule together with an inert gas,  $N_2$ ,  $H_2Se$ , or a mixture thereof. The ZnSe samples were obtained by cleaving the RTHM ingot and have a [110] surface orientation.

Spectroscopic-ellipsometry data were obtained using a commercial SOPRA rotating-polarizer instrument (model ES4G; Seika Corp.) with tracking analyzer over the photon-energy range 1.5–5.3 eV. Measurements were made after cleaning the sample surfaces with methanol. No further procedure was performed for the cleaning of sample surfaces. The spectra were taken at room temperature at the energy intervals of 0.05 eV. The angle of incidence was 75°.

## IV. RESULTS AND DISCUSSION

### A. $\epsilon(\omega)$ spectra

In Fig. 1 we show the dielectric-function spectra  $\epsilon(\omega)$  of ZnSe measured by spectroscopic ellipsometry. These

data were taken without correction for any surface-contamination effect. As seen in the figure, the experimental data reveal clear structures at the 2.7–3.1-eV region. These structures originate from transitions at the  $E_0$  and  $E_0 + \Delta_0$  edges. The structures appearing at the 4.5–5.5-eV region are due to the  $E_1$ -( $E_1 + \Delta_1$ ) transitions.

The model given in Sec. II B can be used to fit the experimental dispersion of  $\epsilon(\omega)$  over most of the spectral range (0–7 eV). The parameters, such as  $A$ ,  $A_{0x}$ , and  $C$ , are commonly used as adjustable constants for the calculations of both  $\epsilon_1(\omega)$  and  $\epsilon_2(\omega)$ . The experimental data of  $\epsilon_1(\omega)$  are, however, usually somewhat larger than our model. In order to improve the fit, we shall therefore also consider a term,  $\epsilon_{1\infty}$ , in addition to  $\epsilon_1(\omega)$ . This term is assumed to be nondispersive and may arise from other higher-lying-gap contributions ( $E'_0$ ,  $E'_1$ ,  $E'_1 + \Delta'_1$ ,  $d_1$ , etc.).

The solid lines are obtained from the sum of Eqs. (1), (3), (6), (7), and  $\epsilon_{1\infty} = 1.2$ . The best-fit parameters are listed in Table II. The vertical arrows in the figure indicate the positions of CP's ( $E_0$  and  $E_0 + \Delta_0$ ) and exciton peak energies ( $E_1 - G_1$  and  $E_1 + \Delta_1 - G_1$ ). Although our experimental photon-energy range did not cover the  $E_2$  CP region ( $\sim 6.7$  eV), we considered its contribution to our  $\epsilon(\omega)$  calculation. This is because the  $E_2$  CP structure provides a peculiar line shape in the  $\epsilon(\omega)$  spectrum even when the photon energies are well below the  $E_2$  CP energy (see Fig. 4 below).

Optical spectra at the  $E_1$  to  $E_1 + \Delta_1$  spectral region of some group-IV elemental and III-V compound semiconductors [Si,<sup>10</sup> Ge,<sup>11</sup>  $\alpha$ -Sn,<sup>13</sup> GaAs,<sup>16</sup> InP,<sup>17</sup> and InSb (Ref. 18)] become sharp when the temperature is lowered. Such spectral change cannot be explained within the framework of the one-electron approximation [i.e., Eq. (4)]. This fact clearly suggests a contribution of excitonic effects to the  $E_1$ -( $E_1 + \Delta_1$ ) transitions. The excitonic effects are usually stronger in II-VI semiconductors than in III-V semiconductors. [This is because of the larger binding energies (smaller values of the static dielectric constant) for the II-VI semiconductors.] We can, there-

TABLE II. Material parameters used in the calculation of optical constants for ZnSe.

Parameter	Numerical value
$E_0$ (eV)	2.69
$E_0 + \Delta_0$ (eV)	3.10
$G_0$ (meV)	17
$A$ (eV <sup>1.5</sup> )	23.4
$A_{0x}$ (eV)	0.03
$\Gamma(E_0 - (E_0 + \Delta_0))$ (meV)	30
$E_1 - G_1$ (eV)	4.75
$E_1 + \Delta_1 - G_1$ (eV)	5.05
$B_{1x}$ (eV)	2.31
$B_{2x}$ (eV)	1.16
$\Gamma(E_1 - (E_1 + \Delta_1))$ (eV)	0.37
$E_2$ (eV)	6.7
$C$	1.6
$\gamma$	0.2
$\epsilon_{1\infty}$	1.2

fore, successfully neglect the one-electron contribution, Eq. (4), to  $\epsilon(\omega)$  in the present analysis. Indeed, Pétroff and Balkanski<sup>58</sup> have analyzed experimental reflectivity spectra of some II-VI semiconductors (CdTe, ZnTe, and ZnSe) and found in the  $E_1-(E_1+\Delta_1)$  region a stronger 2D-exciton peak with extremely weaker one-electron CP structure for CdTe and ZnTe and only a strong 2D-exciton peak for ZnSe.

Pétroff and Balkanski<sup>58</sup> also estimated, from their reflectance spectra, the  $E_1$ -exciton binding energy for CdTe ( $G_1=0.15$  eV) and ZnTe ( $G_1=0.11$  eV). They were, however, not able to determine the value for ZnSe because it was not possible to see the CP in the reflectance spectrum. This can be explained by the fact that for ZnSe the spin-orbit splitting  $\Delta_1$  ( $\sim 0.3$  eV) is nearly equal to the binding energy of the excitons. Thus, the structure of the  $E_1$  CP overlaps with the exciton peak associated with  $E_1+\Delta_1$  transitions. Similarly, we were not able to determine the binding energy  $G_1$  from our spectroscopic-ellipsometry data. However, from the present fitting procedure we can derive the ground-state exciton peak energies to be  $E_1-G_1=4.75$  eV and  $E_1+\Delta_1-G_1=5.05$  eV. Since the 2D ground-state exciton term ( $n=1$ ) contains 95% of the total oscillator strength, we can justifiably neglect the excited-state terms ( $n \geq 2$ ) in the present analysis.

As seen in Fig. 2, the 2D-exciton model of Eq. (6)

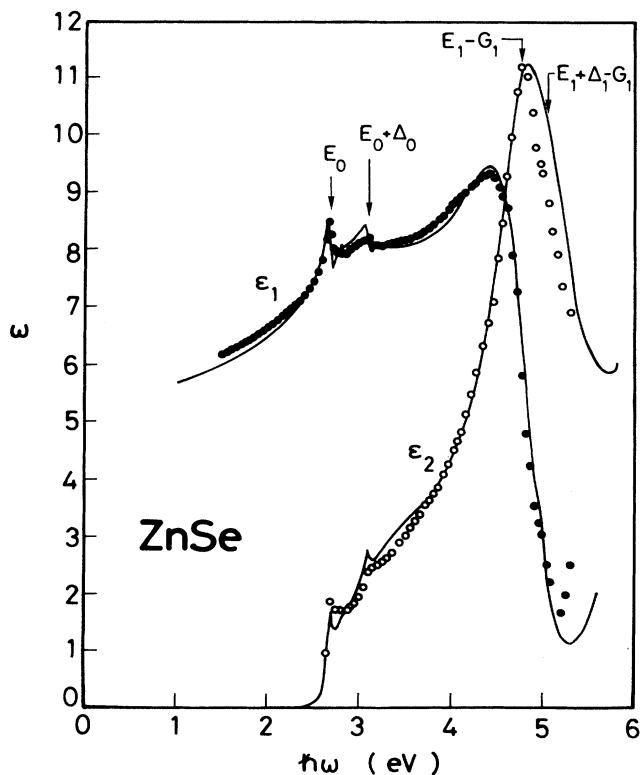


FIG. 2.  $\epsilon(\omega)$  spectrum of ZnSe. The solid ( $\epsilon_1$ ) and open ( $\epsilon_2$ ) circles are the experimental data obtained from ellipsometry measurements. The solid lines are calculated from the sum of Eqs. (1), (3), (6), (7), and  $\epsilon_{1\infty}=1.2$ .

reasonably interprets the strong  $\epsilon_2(\omega)$  peak which is observed at  $\sim 5$  eV. The one-electron [Eq. (1)] and 3D-exciton [Eq. (3)] contributions also explain well the  $\epsilon(\omega)$  spectra at the  $E_0-(E_0+\Delta_0)$  spectral region. Excellent agreement is then achieved between the present theoretical model and experiment over the entire range of photon energies.

Individual contributions to  $\epsilon_2(\omega)$  and  $\epsilon_1(\omega)$  of the various energy gaps for ZnSe are shown in Figs. 3 and 4, respectively. They are obtained from Eq. (1) for the 3D  $M_0$  CP contribution [ $E_0-(E_0+\Delta_0)$ ], from Eq. (3) for the 3D-exciton contribution [ $E_0-(E_0+\Delta)$ ], from Eq. (6) for the 2D-exciton contribution [ $E_1-(E_1+\Delta_1)$ ], and from Eq. (7) for the  $E_2$ -gap contribution.

The  $E_0$  and  $E_0+\Delta_0$  gaps are of the 3D  $M_0$  type. Hence, the line shape of the corresponding  $\epsilon_2(\omega)$  spectrum can be characterized by a continuous absorption obeying the  $\frac{1}{2}$ -power law [i.e.,  $\propto (\hbar\omega-E_0)^{1/2}$ ]. These transitions strongly contribute to the dispersion of  $\epsilon_1(\omega)$  and also to its absolute value. In some III-V compounds, the  $E_0-(E_0+\Delta_0)$  transitions were found to contribute to the dispersion of  $\epsilon_1(\omega)$ , but not to its absolute value.<sup>45,46,49,50,63</sup>

The strength of the  $E_0$  transitions is represented by  $A$  [see Eq. (1)]. This parameter can, in principle, be given by<sup>64</sup>

$$A = \frac{4}{3} \left( \frac{3}{2} m^* \right)^{1.5} P^2, \quad (9)$$

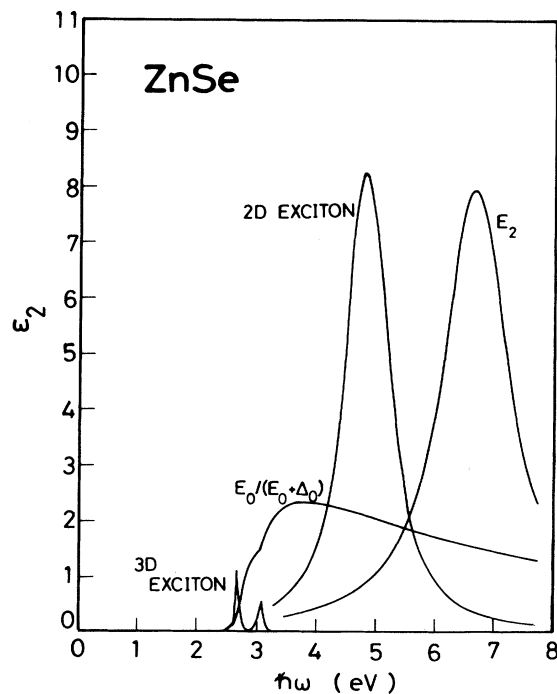


FIG. 3. Individual contributions to  $\epsilon_2(\omega)$  of the various energy gaps for ZnSe. They are obtained from Eq. (1) for the 3D  $M_0$  CP contribution [ $E_0-(E_0+\Delta_0)$ ], from Eq. (3) for the 3D-exciton contribution [ $E_0-(E_0+\Delta)$ ], from Eq. (6) for the 2D-exciton contribution [ $E_1-(E_1+\Delta_1)$ ], and from Eq. (7) for the  $E_2$ -gap contribution.

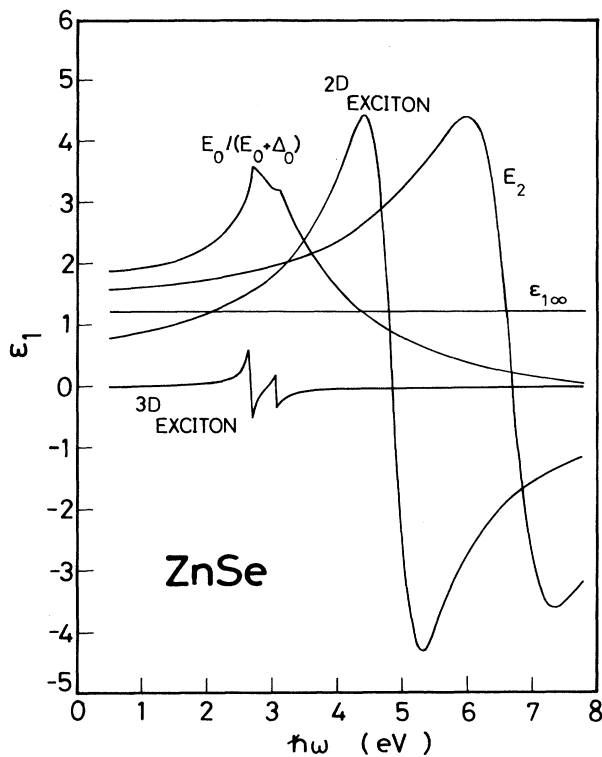


FIG. 4. As Fig. 3, but for  $\epsilon_1(\omega)$ .

where  $m^*$  is the combined density-of-states mass and  $P^2$  is the squared momentum-matrix element. The lowest direct band gap  $E_0$  varies widely from material to material for a family of tetrahedral semiconductors (II-VI and III-V compounds). The larger- $E_0$ -gap material usually has a larger value of the electron effective mass—hence a larger combined density-of-states mass. This simple empirical relation ensures that larger- $E_0$ -gap materials, such as ZnSe, have larger  $E_0$ -gap contribution.<sup>65</sup> In fact, the value for ZnSe ( $A=23.4$ ; see Table II) is considerably larger than those for the III-V compounds, such as GaAs ( $A=3.45$ ), GaSb ( $A=0.71$ ), InP ( $A=6.57$ ), and InAs ( $A=0.61$ ) (see Ref. 49).

The  $E_1$  and  $E_1 + \Delta_1$  gaps should be of the 3D  $M_1$  (or 2D  $M_0$ ) type. Hence, the corresponding one-electron  $\epsilon_2(\omega)$  spectrum [Eq. (4)] should be characterized by a steep low-energy side and a broader high-energy side. The optical response in the  $E_1$ -( $E_1 + \Delta_1$ ) region of III-V semiconductors was successfully interpreted by Eq. (4) with the inclusion of the excitonic effects [i.e., Eq. (6)].<sup>45,47,48,50</sup> As mentioned before, however, the excitonic effects are stronger in II-VI semiconductors than in III-V semiconductors. We can therefore achieve a reasonable fit to the experiment in the  $E_1$ -( $E_1 + \Delta_1$ ) structure region only by considering the 2D-exciton contribution (also see Ref. 51).

We characterized the  $E_2$  structure by the DHO [Eq. (7)]. This model gives a classical Lorentzian line shape. Many-particle effects on CP's in the interband continuum

region of semiconductors have been treated with their detailed electronic energy-band structures.<sup>60,61</sup> Results have shown that the absorption at the  $E_2$  CP is markedly weakened with no drastic change in its shape by the introduction of the excitonic interaction. Unfortunately, however, it seems that no analytical line shape suitable to fit the exciton-affected  $E_2$  line shape has been reported to date. We found that, for InP (Ref. 48) and GaAs,<sup>50</sup> the DHO model is a good representation for the  $E_2$  ( $E'_0$ ) CP both with and without the presence of the excitonic interaction.

### B. Refractive index, extinction coefficient, and absorption coefficient

Optical spectra, such as the refractive index, the absorption coefficient, and the normal-incidence reflectivity, can be easily obtained from the present study in the form of practical functions, since they are directly related to the dielectric function  $\epsilon(\omega)$ .<sup>47,49</sup>

Figure 5 shows the numerically calculated spectral dependence of the real refractive index  $n$  and the extinction coefficient  $k$  for ZnSe (solid lines). The solid ( $n$ ) and open ( $k$ ) circles are the experimental data obtained by spectroscopic ellipsometry. The strongest peak in  $n$  at  $\sim 4.5$  eV is related mainly to the 2D-exciton transitions [ $E_1$ -( $E_1 + \Delta_1$ )]. The relatively weak  $E_0$  and  $E_0 + \Delta_0$  structures are also clearly seen in the 2.7–3.1-eV spectral region. The  $k$  above 2.6 eV is associated with the onset of the  $E_0$ -gap transitions and that one above 4.5 eV is associated with the 2D-exciton transitions ( $E_1$  CP). It is clear that our theoretical model agrees quite well with the

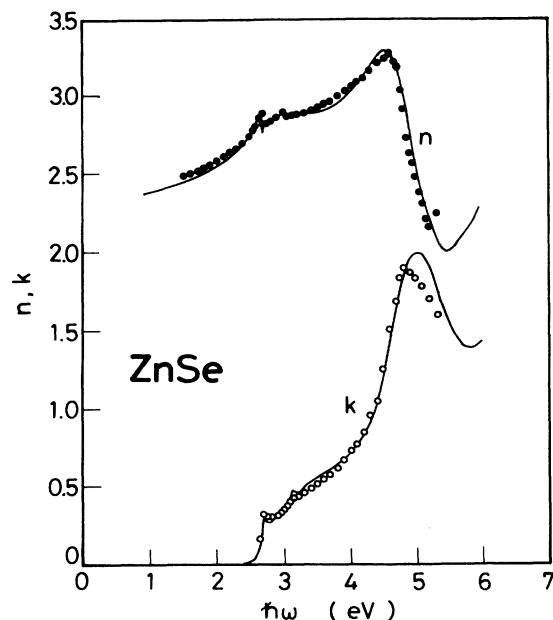


FIG. 5. Numerically calculated spectral dependence of the real refractive index  $n$  and the extinction coefficient  $k$  for ZnSe (solid lines). The solid ( $n$ ) and open ( $k$ ) circles are the experimental data.

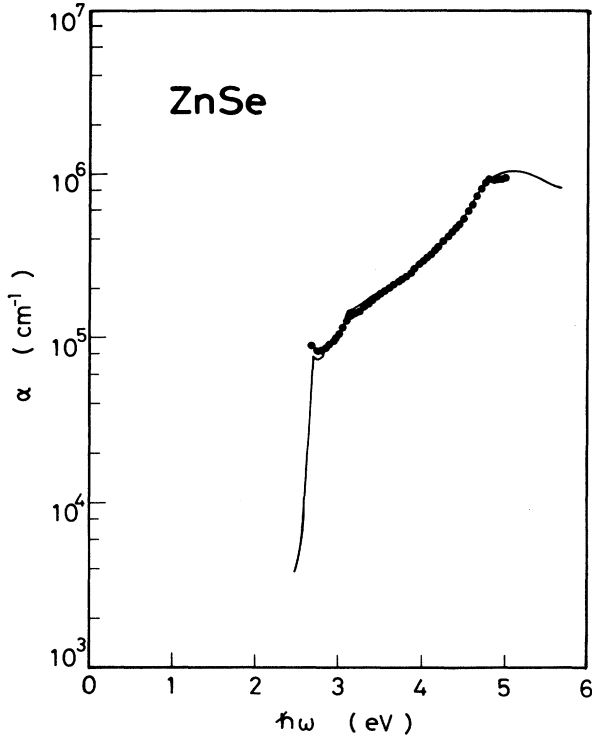


FIG. 6. Comparison of our calculated absorption coefficient  $\alpha$  (solid line) to the experimental data for ZnSe.

experimental  $n$  and  $k$  over a wide range of photon energy.

A comparison of our calculated absorption coefficient  $\alpha$  (solid line) to the experimental data for ZnSe is shown in Fig. 6. Like  $n$  and  $k$ , the absorption data  $\alpha$  reveal the presence of weak structures related to the  $E_0$  and  $E_0 + \Delta_0$  transitions (2.7–3.1 eV). The absorption in the high-energy region is associated with the strong 2D-exciton transitions.

### C. Refractive-index dispersion in the transparency region

A number of semiempirical models have been proposed in past years to model the refractive index of semiconductors below the lowest direct band gap.<sup>66</sup> Such information forms an important part in the design of various optoelectronic devices. As seen in Fig. 2 (Fig. 5), the agreement between our model and the experimental  $\epsilon_1$  ( $n$ ) data seems to be reasonably good over the entire range of photon energies, but in the transparency region the agreement is not so good.

Figure 7 shows the measured refractive-index dispersion for ZnSe at photon energies below the  $E_0 + \Delta_0$  gap. Since the  $E_2$ -gap contribution is nearly constant in the low-photon-energy region (see Fig. 4), it is possible to account for it with the nondispersive term  $\epsilon_{1\infty}$ . The resulting model does not give a satisfactory fit to the experimental data at higher photon energies ( $> 2.7$  eV), but gives an excellent fit at lower photon energies (trans-

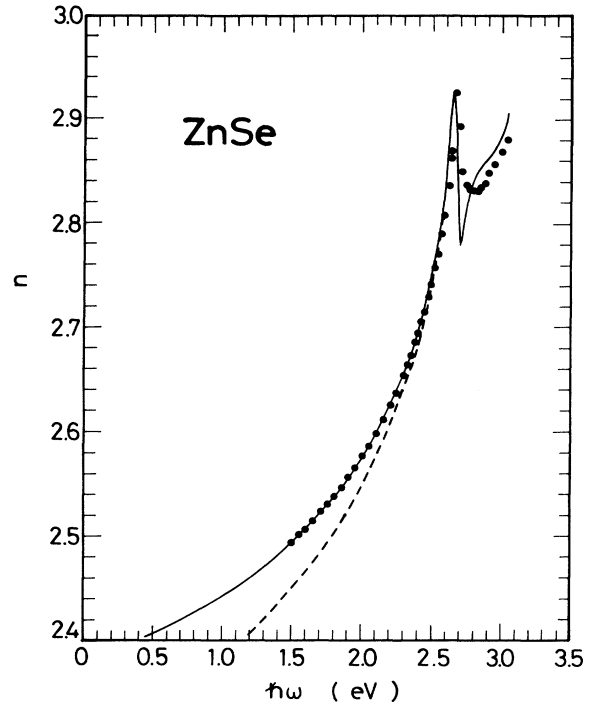


FIG. 7. Measured refractive-index dispersion for ZnSe at photon energies below the  $E_0 + \Delta_0$  gap (solid circles). The solid line is calculated from the sum of Eqs. (1), (3), (6), and  $\epsilon_{1\infty} = 3.1$ . The dashed line is also the result of the sum of Eqs. (1), (3), (6), (7), and  $\epsilon_{1\infty} = 1.2$  [same as that seen in Fig. 2 (solid line)].

parency region). This calculated result is shown in Fig. 7 by the solid line. The CP-parameter values for the  $E_0$ - ( $E_0 + \Delta_0$ )- and  $E_1$ - ( $E_1 + \Delta_1$ )-gap transitions are the same as those used in Fig. 2 (see Table II) except  $\epsilon_{1\infty}$ . The dashed line is also the result of the sum of Eqs. (1), (3), (6), (7), and  $\epsilon_{1\infty} = 1.2$  [same as that seen in Fig. 2 (solid line)]. The  $\epsilon_{1\infty}$  value used here is 3.1 which is considerably larger than that obtained in Fig. 2 ( $= 1.2$ ). The increase in  $\epsilon_{1\infty}$  is due to the addition of the  $E_2$ -gap contribution to it. The figure shows that the agreement between our model and the experiment in the region below the fundamental absorption edge is very good. Similarly, Strössner, Ves, and Cardona<sup>67</sup> have shown that the refractive-index dispersion below and near the direct band gap of GaP can be very well described with a model that does not take into account the  $E_2$ -gap contribution. A similar conclusion on AISb has also been reached by Zollner *et al.*<sup>20</sup>

Below the reststrahlen range, the real part of the dielectric constant asymptotically approaches the static dielectric constant ( $\epsilon_s$ ). The optical constant connecting the reststrahlen–near-infrared range is called the high-frequency dielectric constant ( $\epsilon_\infty$ ). Measurements of the dielectric constant  $\epsilon_\infty$  of ZnSe have yielded widely different values ranging from 5.4 to 6.1 (see Table III). As  $\hbar\omega \rightarrow 0$ , the electronic contribution to the optical dielectric constant approaches a limiting value,  $\epsilon_1 \rightarrow \epsilon_\infty$ . We can estimate from our present theoretical model the

TABLE III. Static ( $\epsilon_s$ ) and high-frequency ( $\epsilon_\infty$ ) dielectric constants of ZnSe.

$\epsilon_s$	$\epsilon_\infty$	Ref.
8.1	5.75	a
9.1		b
	5.90	c
7.6	5.4	d
9.2	6.1	e
9.25		f
8.6	5.7	g

<sup>a</sup>M. Aven *et al.*, J. Appl. Phys. (Suppl.) **32**, 2261 (1961).

<sup>b</sup>D. Berlincourt *et al.*, Phys. Rev. **129**, 1009 (1963).

<sup>c</sup>D. T. F. Marple, J. Appl. Phys. **35**, 539 (1964).

<sup>d</sup>A. Mitsuishi, in U.S.-Japan Cooperative Seminar on Far Infrared Spectroscopy, Columbus, Ohio, 1965 (unpublished).

<sup>e</sup>S. S. Nitra, J. Phys. Soc. Jpn (Suppl.) **21**, 67 (1966).

<sup>f</sup>I. Strzalkowski *et al.*, Appl. Phys. Lett. **28**, 350 (1976).

<sup>g</sup>Present work.

value of  $\epsilon_\infty$  to be 5.7. The  $\epsilon_s$  and  $\epsilon_\infty$  are related to the long-wavelength phonon frequencies,  $\omega_{LO}$  (longitudinal optical) and  $\omega_{TO}$  (transverse optical), by the generalized Lyddane-Sachs-Teller relation

$$\epsilon_s/\epsilon_\infty = (\omega_{LO}/\omega_{TO})^2. \quad (10)$$

Introducing  $\omega_{LO} = 251 \text{ cm}^{-1}$ ,  $\omega_{TO} = 204 \text{ cm}^{-1}$  (Ref. 68),

and  $\epsilon_\infty = 5.7$  into Eq. (10), we obtain 8.6 for the value of  $\epsilon_s$ . This value also falls in the range 7.6–9.2 reported in Table III.

## V. CONCLUSIONS

We have measured the real ( $\epsilon_1$ ) and imaginary ( $\epsilon_2$ ) parts of the dielectric function of ZnSe by spectroscopic ellipsometry in the 1.5–5.3-eV photon-energy range at room temperature. The observed spectra reveal distinct structures at energies of the  $E_0$ ,  $E_0 + \Delta_0$ ,  $E_1$ , and  $E_1 + \Delta_1$  critical points (CP's). These data are analyzed on the basis of a simplified model of the interband transitions. The model includes the  $E_0$ ,  $E_0 + \Delta_0$ ,  $E_1$ ,  $E_1 + \Delta_1$ , and  $E_2$  transitions as the main dispersion mechanisms. Since excitonic effects may profoundly modify the CP singularity structure, the model is made to account both for the one-electron feature and the excitons at these CP's. Our results are in satisfactory agreement with the experimental data over the entire range of photon energies. Dielectric-function-related optical data of ZnSe, such as the refractive index, the extinction coefficient, and the absorption coefficient, are also presented and analyzed.

## ACKNOWLEDGMENTS

One of us (S. A.) acknowledges financial support from the Gunma University Foundation for Science and Technology, Gunma, Japan.

<sup>1</sup>M. Cardona, J. Appl. Phys. (Suppl.) **32**, 2151 (1961).

<sup>2</sup>M. Aven, D. T. F. Marple, and B. Segall, J. Appl. Phys. (Suppl.) **32**, 2261 (1961).

<sup>3</sup>M. Cardona and G. Harbeke, J. Appl. Phys. **34**, 813 (1963).

<sup>4</sup>E. Matatagai, A. G. Thompson, and M. Cardona, Phys. Rev. **176**, 950 (1968).

<sup>5</sup>Y. Pétrouff, M. Balkanski, J. P. Walter, and M. L. Cohen, Solid State Commun. **7**, 459 (1969).

<sup>6</sup>J. P. Walter, M. L. Cohen, Y. Pétrouff, and M. Balkanski, Phys. Rev. B **1**, 2661 (1970).

<sup>7</sup>J. L. Freeouf, Phys. Rev. B **7**, 3810 (1973).

<sup>8</sup>D. E. Aspnes, in *Optical Properties of Solids: New Developments*, edited by B. O. Seraphin (North-Holland, Amsterdam, 1976), p. 799.

<sup>9</sup>D. E. Aspnes and A. A. Studna, Phys. Rev. B **27**, 985 (1983).

<sup>10</sup>P. Lautenschlager, M. Garriga, L. Viña, and M. Cardona, Phys. Rev. B **36**, 4821 (1987).

<sup>11</sup>L. Viña, S. Logothetidis, and M. Cardona, Phys. Rev. B **30**, 1979 (1984).

<sup>12</sup>J. Humlíček, M. Garriga, M. I. Alonso, and M. Cardona, J. Appl. Phys. **65**, 2827 (1989).

<sup>13</sup>L. Viña, H. Höchst, and M. Cardona, Phys. Rev. B **31**, 958 (1985).

<sup>14</sup>S. M. Kelso, D. E. Aspnes, M. A. Pollack, and R. E. Nahory, Phys. Rev. B **26**, 6669 (1982).

<sup>15</sup>D. E. Aspnes, S. M. Kelso, R. A. Logan, and R. Bhat, J. Appl. Phys. **60**, 754 (1986).

<sup>16</sup>P. Lautenschlager, M. Garriga, S. Logothetidis, and M. Cardona, Phys. Rev. B **35**, 9174 (1987).

<sup>17</sup>P. Lautenschlager, M. Garriga, and M. Cardona, Phys. Rev. B

**36**, 4813 (1987).

<sup>18</sup>S. Logothetidis, L. Viña, and M. Cardona, Phys. Rev. B **31**, 947 (1985).

<sup>19</sup>M. Garriga, P. Lautenschlager, M. Cardona, and K. Ploog, Solid State Commun. **61**, 157 (1987).

<sup>20</sup>S. Zollner, C. Lin, E. Schönherr, A. Böhringer, and M. Cardona, J. Appl. Phys. **66**, 383 (1989).

<sup>21</sup>S. Logothetidis, M. Cardona, P. Lautenschlager, and M. Cardona, Phys. Rev. B **34**, 2458 (1986).

<sup>22</sup>P. Lautenschlager, S. Logothetidis, L. Viña, and M. Cardona, Phys. Rev. B **32**, 3811 (1985).

<sup>23</sup>K. Kumazaki, L. Viña, C. Umbach, and M. Cardona, Phys. Status Solidi B **156**, 371 (1989).

<sup>24</sup>M. L. Cohen and T. K. Bergstresser, Phys. Rev. **141**, 789 (1966).

<sup>25</sup>D. J. Stukel, R. N. Euwema, T. C. Collins, F. Herman, and R. L. Kortum, Phys. Rev. **179**, 740 (1969).

<sup>26</sup>F. Cerdeira, J. S. DeWitt, U. Rössler, and M. Cardona, Phys. Status Solidi **41**, 735 (1970).

<sup>27</sup>J. Chelikowsky, D. J. Chadi, and M. L. Cohen, Phys. Rev. B **8**, 2786 (1973).

<sup>28</sup>J. R. Chelikowsky and M. L. Cohen, Phys. Rev. B **14**, 556 (1976).

<sup>29</sup>C. S. Wang and B. M. Klein, Phys. Rev. B **24**, 3417 (1981).

<sup>30</sup>J. E. Bernard and A. Zunger, Phys. Rev. B **36**, 3199 (1987).

<sup>31</sup>R. W. Jansen and O. F. Sankey, Phys. Rev. B **36**, 6520 (1987).

<sup>32</sup>M. Cardona, N. E. Christensen, and G. Fasol, Phys. Rev. B **38**, 1806 (1988).

<sup>33</sup>A. Continenza, S. Massidda, and A. J. Freeman, Phys. Rev. B **38**, 12996 (1988).

- <sup>34</sup>J. R. Chelikowsky, T. J. Wagener, J. H. Weaver, and A. Jin, *Phys. Rev. B* **40**, 9644 (1989).
- <sup>35</sup>Y. Li and P. J. Lin-Chung, *Phys. Status Solidi B* **153**, 215 (1989).
- <sup>36</sup>F. H. Pollak, in *II-IV Semiconducting Compounds*, edited by D. G. Thomas (Benjamin, New York, 1967), p. 552.
- <sup>37</sup>G. E. Hite, D. T. F. Marple, M. Aven, and B. Segall, *Phys. Rev.* **156**, 850 (1967).
- <sup>38</sup>S. Fujiwara, K. Hattori, and M. Fukai, *Phys. Lett.* **31A**, 258 (1970).
- <sup>39</sup>A. M. Andriesh, B. T. Kolomiets, É. A. Senokosov, and Sh. M. Efendiev, *Fiz. Tekh. Poluprovodn.* **4**, 1372 (1971) [*Sov. Phys. Semicond.* **4**, 1165 (1971)].
- <sup>40</sup>L. Ley, R. A. Pollak, F. R. McFeely, S. P. Kowalczyk, and D. A. Shirley, *Phys. Rev. B* **9**, 600 (1974).
- <sup>41</sup>D. E. Eastman, W. D. Grobman, J. L. Freeouf, and M. Erbudak, *Phys. Rev. B* **9**, 3473 (1974).
- <sup>42</sup>J. Krauser, D. Theis, and H. -E. Gumlich, *Phys. Lett.* **51A**, 119 (1975).
- <sup>43</sup>P. Jaszczyn-Kopec, B. Canny, G. Syfosse, and G. Hamel, *Solid State Commun.* **49**, 795 (1984).
- <sup>44</sup>S. Ves, K. Strössner, N. E. Christensen, C. K. Kim, and M. Cardona, *Solid State Commun.* **56**, 479 (1985).
- <sup>45</sup>S. Adachi, *Phys. Rev. B* **41**, 3504 (1990).
- <sup>46</sup>S. Adachi, *Phys. Rev. B* **35**, 7454 (1987); **38**, 12 345 (1988); **38**, 12 966 (1988); **39**, 12 612 (1989).
- <sup>47</sup>S. Adachi, *J. Appl. Phys.* **66**, 813 (1989); **66**, 3224 (1989); **67**, 6427 (1990).
- <sup>48</sup>S. Adachi, *Jpn. J. Appl. Phys.* **28**, 1536 (1989).
- <sup>49</sup>S. Adachi, *J. Appl. Phys.* **66**, 6030 (1989).
- <sup>50</sup>S. Adachi, *Phys. Rev. B* **41**, 1003 (1990).
- <sup>51</sup>S. Adachi, *J. Appl. Phys.* **68**, 1192 (1990).
- <sup>52</sup>R. J. Elliott, *Phys. Rev.* **108**, 1384 (1957).
- <sup>53</sup>H. Venghaus, *Phys. Rev. B* **19**, 3071 (1979).
- <sup>54</sup>D. W. Jenkins, *J. Appl. Phys.* **68**, 1848 (1990).
- <sup>55</sup>B. Velický and J. Sak, *Phys. Status Solidi* **16**, 147 (1966).
- <sup>56</sup>E. O. Kane, *Phys. Rev.* **180**, 852 (1969).
- <sup>57</sup>J. E. Rowe and D. E. Aspnes, *Phys. Rev. Lett.* **25**, 162 (1970).
- <sup>58</sup>Y. Pétroff and M. Balkanski, *Phys. Rev. B* **3**, 3299 (1971).
- <sup>59</sup>S. Antoci and G. F. Nardelli, *Phys. Rev.* **6**, 1311 (1972).
- <sup>60</sup>M. del Castillo-Mussot and L. J. Sham, *Phys. Rev. B* **31**, 2092 (1985).
- <sup>61</sup>W. Hanke and L. J. Sham, *Phys. Rev. B* **21**, 4656 (1980).
- <sup>62</sup>T. Taguchi, I. Kidoguchi, and H. Nanba, U.S. Patent No. 4,866,007.
- <sup>63</sup>S. Adachi, *J. Appl. Phys.* **61**, 4869 (1987).
- <sup>64</sup>P. Y. Yu and M. Cardona, *J. Phys. Chem. Solids* **34**, 29 (1973).
- <sup>65</sup>S. Adachi, *J. Appl. Phys.* **53**, 5863 (1982).
- <sup>66</sup>A. N. Pikhtin and A. D. Yas'kov, *Fiz. Tekn. Poluprovodn.* **22**, 969 (1988) [*Sov. Phys. Semicond.* **22**, 613 (1988)].
- <sup>67</sup>K. Strössner, S. Ves, and M. Cardona, *Phys. Rev. B* **32**, 6614 (1985).
- <sup>68</sup>J. L. Lewis, R. L. Wadsack, and R. K. Chang, in *Light Scattering in Solids*, edited by M. Balkanski (Flammarion, Paris, 1971), p. 41.